Evaluation of breast tumor margins *in vivo* with intraoperative photoacoustic imaging

Lei Xi,[1] Stephen R. Grobmyer,[2] Lei Wu,[3] Ruimin Chen,[4] Guangyin Zhou,[2] Luke G. Gutwein,[2] Jingjing Sun,[3] Wenjun Liao,[3] Qifa Zhou,[4] Huikai Xie,[3] and Huabei Jiang[1,*]

[1]*Department of Biomedical Engineering, University of Florida, Gainesville, FL 32611, USA*
[2]*Department of Surgery, University of Florida, Gainesville, FL 32611, USA*
[3]*Department of Electrical and Computer Engineering, University of Florida, Gainesville, FL 32611, USA*
[4]*Department of Biomedical Engineering, University of Southern California, Los Angeles, CA 90089, USA*
[*]*hjiang@bme.ufl.edu*

Abstract: The use of photoacoustic effect is a promising approach for biomedical imaging in living tissues. Photoacoustic tomography (PAT) has been demonstrated to image breast cancer, brain vasculature, arthritis and seizure focus owing to its rich optical contrast and high resolution in a single imaging modality. Here we report a microelectromechanical systems (MEMS)-based intraoperative PAT (iPAT) technique, and demonstrate its ability to accurately map tumors in three-dimension and to inspect the completeness of tumor resection during surgery in a tumor-bearing mouse model. The MEMS imaging probe is small and has the potential to be conveniently used to guide surgical resection of tumors in the breast.

OCIS codes: (170.5120) Photoacoustic imaging; (170.0110) Imaging systems.

References and links

1. A. Jemal, R. Siegel, E. Ward, Y. Hao, J. Xu, T. Murray, and M. J. Thun, "Cancer statistics, 2008," CA Cancer J. Clin. **58**(2), 71–96 (2008).
2. American Cancer Society, Cancer facts and Figs. 2009 American cancer society, Atlanta, 2009.
3. American Cancer Society, Cancer facts and Figs. 2010 American cancer society, Atlanta, 2010.
4. A. Taghian, M. Mohiuddin, R. Jagsi, S. Goldberg, E. Ceilley, and S. Powell, "Current perceptions regarding surgical margin status after breast-conserving therapy: results of a survey," Ann. Surg. **241**(4), 629–639 (2005).
5. L. Assersohn, T. J. Powles, S. Ashley, A. G. Nash, A. J. Neal, N. Sacks, J. Chang, U. Querci della Rovere, and N. Naziri, "Local relapse in primary breast cancer patients with unexcised positive surgical margins after lumpectomy, radiotherapy and chemoendocrine therapy," Ann. Oncol. **10**(12), 1451–1455 (1999).
6. G. C. Balch, S. K. Mithani, J. F. Simpson, and M. C. Kelley, "Accuracy of intraoperative gross examination of surgical margin status in women undergoing partial mastectomy for breast malignancy," Am. Surg. **71**(1), 22–27, discussion 27–28 (2005).
7. B. Sigal-Zafrani, J. S. Lewis, K. B. Clough, A. Vincent-Salomon, A. Fourquet, M. Meunier, M. C. Falcou, and X. Sastre-Garau; Institut Curie Breast Study Group, "Histological margin assessment for breast ductal carcinoma in situ: precision and implications," Mod. Pathol. **17**(1), 81–88 (2004).
8. F. Meric, N. Q. Mirza, G. Vlastos, T. A. Buchholz, H. M. Kuerer, G. V. Babiera, S. E. Singletary, M. I. Ross, F. C. Ames, B. W. Feig, S. Krishnamurthy, G. H. Perkins, M. D. McNeese, E. A. Strom, V. Valero, and K. K. Hunt, "Positive surgical margins and ipsilateral breast tumor recurrence predict disease-specific survival after breast-conserving therapy," Cancer **97**(4), 926–933 (2003).
9. H. Jiang, *Diffuse Optical Tomography: Principles and Applications* (CRC Press, 2011).
10. S. Manohar, A. Kharine, J. C. G. van Hespen, W. Steenbergen, and T. G. van Leeuwen, "Photoacoustic mammography laboratory prototype: imaging of breast tissue phantoms," J. Biomed. Opt. **9**(6), 1172–1181 (2004).
11. L. V. Wang, "Multiscale photoacoustic microscopy and computed tomography," Nat. Photonics **3**(9), 503–509 (2009).
12. A. A. Oraevsky, S. A. Ermilov, A. Conjusteau, T. Miller, R. R. Lacewell, K. Mehta, D. Herzog, S. Thompson, A. Stein, T. Khamapirad, M. McCorvey, and P. Otto, "Initial clinical evaluation of laser optoacoustic imaging system for diagnostic imaging of breast cancer," Breast Cancer Res. Treat. **106**, S47 (2007).
13. R. A. Kruger, K. D. Miller, H. E. Reynolds, W. L. Kiser, Jr., D. R. Reinecke, and G. A. Kruger, "Breast cancer in vivo: contrast enhancement with thermoacoustic CT at 434 MHz-feasibility study," Radiology **216**(1), 279–283 (2000).

14. C. Kim, K. H. Song, F. Gao, and L. V. Wang, "Sentinel lymph nodes and lymphatic vessels: noninvasive dual-modality in vivo mapping by using indocyanine green in rats--volumetric spectroscopic photoacoustic imaging and planar fluorescence imaging," Radiology **255**(2), 442–450 (2010).
15. T. N. Erpelding, C. Kim, M. Pramanik, L. Jankovic, K. Maslov, Z. Guo, J. A. Margenthaler, M. D. Pashley, and L. V. Wang, "Sentinel lymph nodes in the rat: noninvasive photoacoustic and US imaging with a clinical US system," Radiology **256**(1), 102–110 (2010).
16. Q. Zhou, X. Xu, E. Gottlieb, L. Sun, J. M. Cannata, H. Ameri, M. S. Humayun, P. Han, and K. K. Shung, "PMN-PT single crystal high frequency ultrasonic needle transducers for pulsed wave doppler application," IEEE Trans. Ultrason., Ferroelec, Freq. Control **54**(3), 668–675 (2007).
17. L. Wu and H. Xie, "A large vertical displacement electrothermal bimorph microactuator with very small lateral shift," Sens. Actuators A Phys. **145–146**, 371–379 (2008).
18. J. M. Yang, K. Maslov, H. C. Yang, Q. Zhou, K. K. Shung, and L. V. Wang, "Photoacoustic endoscopy," Opt. Lett. **34**(10), 1591–1593 (2009).
19. R. L. Shelton and B. E. Applegate, "Off-axis photoacoustic microscopy," IEEE Trans. Biomed. Eng. **57**(8), 1835–1838 (2010).

1. Introduction

Breast cancer remains a major public health problem affecting 1 in 4 women in the U.S [1]. As a result of population based screening programs for breast cancer, most women are currently diagnosed with early stage breast cancer in the U.S [1–3]. In a lumpectomy, margin is typically examined using pathological methods to determine if there is at least 2 mm of surrounding normal breast tissue beyond the tumor border; this is considered to be a negative margin. However, if the tumor cells come to the edge of the resected tissue, it is considered to be a positive margin [4, 5].

Methods currently available for intraoperative margin assessment, such as gross examination, frozen section, ultrasound, and touch-prep, have various limitations with false-negative diagnoses in 20 to 50% of the patients [6–8]. Therefore, there is an urgent need to develop sensitive and accurate intraoperative methods for detecting tumor margins in order to reduce tumor recurrence and to improve the survival rate of breast cancer patients.

Laser-induced photoacoustic tomography (PAT), where a single short-pulsed light beam illuminates an object and the photoacoustic waves excited by thermoelastic expansion are measured using wideband ultrasound transducer(s), retains the desired high optical contrast/sensitivity while providing much improved spatial resolution than pure optical tomographic methods by detecting less-scattering ultrasonic waves. To date several clinical studies have been reported to evaluate the feasibility of PAT for breast cancer detection [9–15].

The purpose of the current work is to evaluate high resolution imaging of tumor margins and resection inspection by using an intraoperative photoacoutic imaging system. The penetration depth for our intraoperative photoacoutic imaging system is 2.3mm which is clinically relevant for tumor margin assessment of lumpectomy specimen. We demonstrate this technique using a tumor-bearing animal model. The results obtained show accurate correlation with the histology.

2. Intraoperative photoacoutc tomography (iPAT) system

In our microelectromechanical system (MEMS) based photoacoutc imaging system, short laser pulses of 6 nanosecond duration are generated from a Nd:YAG 532 nm laser (NL 303HT from EKSPLA, Lithuania), and a reflection mirror is employed to deliver light into a miniaturized probe (Fig. 1(a)). Inside the probe, there are an aperture (for generating a 0.2 mm-diameter light spot), a wedge-shaped mirror (Fig. 1(c)) and a MEMS mirror (Fig. 1(b)). A custom designed PZT (DL-53HD, DeL Piezo Specialties, LLC, Wellington, FL) ultrasound transducer [16] (unfocused ring-shape, 5.5 MHz central frequency, 7mm inner diameter and 11.5mm outer diameter) is attached to the end of the probe to detect photoacoustic waves.

A MEMS mirror based on electrothermal bimorph actuation is utilized to realize two-dimensional light scanning [17]. The moveable mirror plate (Fig. 1(b)) is as large as 0.8 mm $\times$ 0.8 mm in a 2 mm $\times$ 2 mm device footprint. The MEMS mirror is fixed on a ramp with

an angle of 22.5° (Fig. 1(d)), allowing light to scan from position 3 to position 4 (Fig. 1(c)), while the MEMS mirror moves from position 1 to position 2. The measured vertical resonant frequency is 500 Hz. In Media 1 online, four channels of voltage signals are utilized to drive four actuators (Fig. 1(b)) of the MEMS mirror.

The capability of our iPAT system was validated by mouse experiments involving tumor extirpation (n = 8). The laser beam illuminated the tumor surface along Z axis at an energy density of 8 mJ/cm^2 that is lower than the American National Standards Institute safety limit of 20 mJ/cm^2. Two 0~4 V ramp signals with repetition frequency of 0.1 Hz were used to drive two actuators moving along Y axis and the other two signals with the same magnitude but different repetition frequency of 0.002 Hz were used to drive the actuators moving along X axis. The photoacoustic signals were recorded without averaging at 10Hz frame rates, amplified and converted to a one-dimensional (1D) image assuming a constant ultrasound velocity in soft tissue (1.54 mm/µs). A square area (10 mm × 10 mm) in XY plane was imaged to produce a 3D image of the tissue volume.
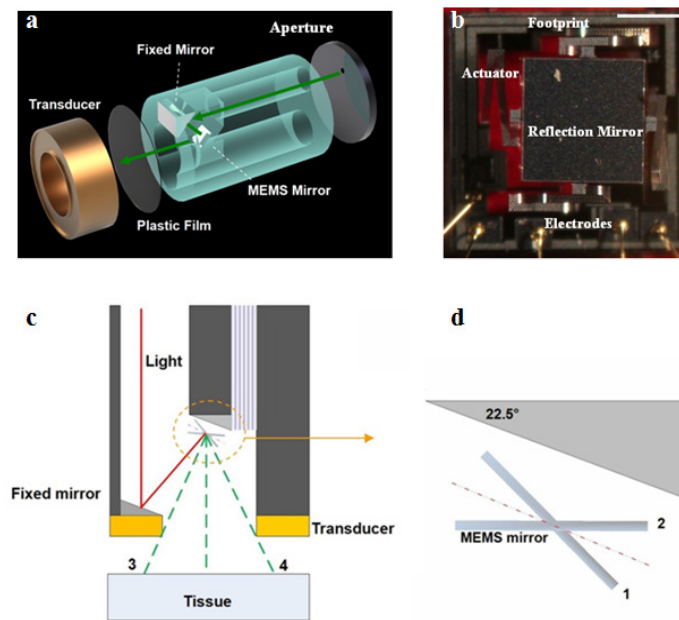

Fig. 1. Schematic representation of the MEMS probe. (a) 3D rendering of the probe (b) Photograph of the MEMS mirror with four actuators and five pads bonded with gold wire (Media 1). (c) Schematic of the miniaturized probe. A wedge-shaped mirror plated with aluminum is fixed in position to redirect the light beam to the MEMS mirror. (d) The MEMS mirror is fixed on a ramp with an angle of 22.5°

One set of data measured from a cylindrical phantom with Ink covering the imaged surface was used to calibrate all the experimental data used in this study to reduce the effect of focal signal from the center area from the ring-shaped transducer. All slices were processed and displayed by normalizing the images to the same scale (0-256) with a threshold (−6dB level of the normalized peak photoacoustic signal) [18].

3. Results

A 100µm diameter tissue mimicking target (absorption coefficient μ_a = 0.049mm^{-1}, reduced scattering coefficient μ_s' = 0.5 mm^{-1}) embedded in turbid media (μ_a = 0.012mm^{-1}, μ_s' = 0.35 mm^{-1}) was imaged. Chicken breast with thickness of up to 2.3mm was added to investigate the resolution and signal-noise ratio versus target position [18].

In Fig. 2(a), the system's axial and transverse resolutions are plotted versus the target's position. The experimental axial resolution (black crosses), determined by the bandwidth of transducer, varied from 0.36 to 0.4mm which agrees well with the theoretical value of 0.3 to 0.35mm [19]. The experimental transverse resolution (blue dots), based on the size of light spot, decreased from 0.24 to 0.96mm when the depth increased. Again this is consistent with the theoretical depth-dependent transverse resolution of 0.21~0.95mm (red dots). The signal-to-noise ratio (SNR) measured in turbid media is shown in Fig. 2(b), decreasing from 32 dB to 18 dB within 2.3mm.
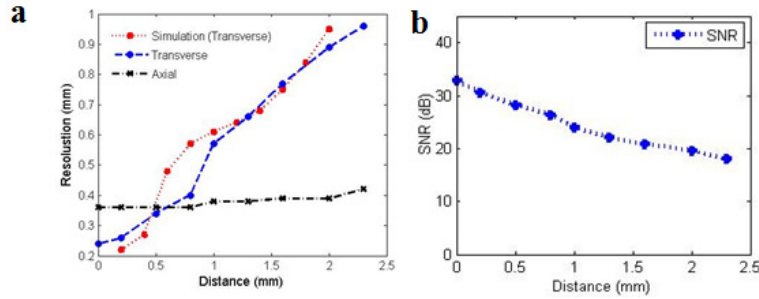

Fig. 2. Performance of this system. (a) Axial and transverse resolutions versus target depth. (b) Signal-to-noise ratio (SNR) versus target depth.
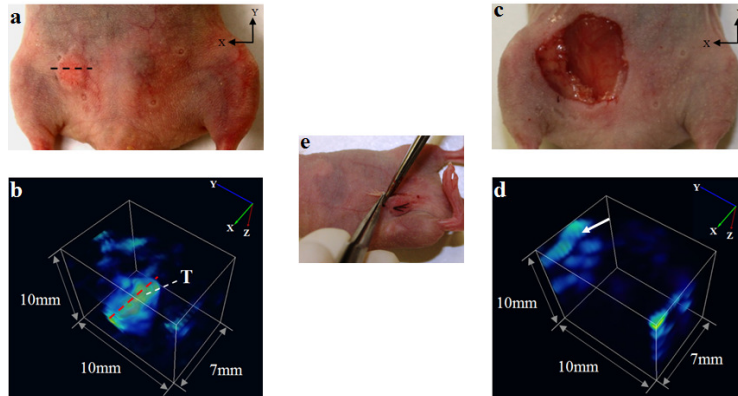

Fig. 3. *In vivo* three-dimensional (3D) tumor mapping in a mouse model. (a) Photograph of the mouse with tumor implanted in abdomen before surgery. (b) In vivo 3D photoacoustic image (Media 2). The distance shown along Z axis includes the tumor depth and the distance between the surface of transducer and mouse skin. (c) Photograph of the mouse after tumor resection. (d) 3D photoacoustic image of the tumor cavity after surgery to examine the completeness of the tumor resection. (e) Photograph of the tumor resection guided by 3D photoacoustic image shown in b.

The volumetric shape, size and position of the tumor are shown in Fig. 3(b) (see Media 2 for multi-view 3D image). The surgeon removed the tumor marked with "T" in Fig. 3(b). In these experiments, the line of surgical resection of tumor was intentionally carried out beyond the margin of the imageable tumor, consistent with clinical practice. After the surgical procedure, the surgical area shown in Fig. 3(c) was inspected again by the same imaging method to ensure the complete resection of tumor. The image shown in Fig. 3(d) confirmed the completed resection of tumor. The signal (indicated by the arrow in Fig. 3(d)) was from the inner surface of the ring-shaped transducer. This signal disappeared in Fig. 3(b) due to strong signals from the tumor and normalized image procedure was used.

Following tumor removal, the tumor size as determined by iPAT was compared with the actual tumor size as measured histologically. Hematoxylin and eosin (H&E) stained sections

along XZ plane were obtained after the photoacoustic experiments. A 2D PAT slice along the red dashed line in Fig. 3(b) was selected and compared with the corresponding H&E stained section (the black dashed line in Fig. 3(a)) as shown in Figs. 4(a) and 4(b). Figure 4(c) shows the photograph of the tumor in comparison with the H&E and PAT slices. Also, the red dashed line along the top margin of the tumor shown in Fig. 4(a) matches well with the top margin (black dashed line in Fig. 4(b)) of the H&E section and photograph (red dashed line in Fig. 4(c)). The size along two typical directions (Lines 1 and 2 in Fig. 4(a)) was estimated to be 2.1 and 1.2 mm, respectively, in excellent agreement with the actual dimensions of 2.2 and 1.1 mm measured from the histology slice (Lines 1′ and 2′ in Fig. 4(b)). Such comparisons were applied to other two H&E staining sections along XZ plane for this mouse, and we found that the measured error was less than 8.5% for all three slices.
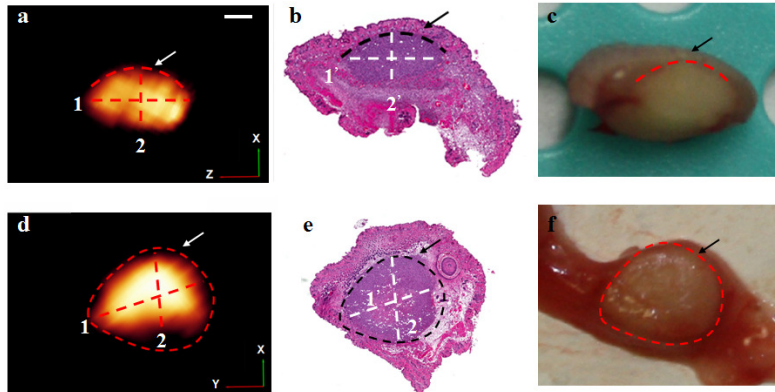

Fig. 4. Quantitative analysis of the photoacoustic slices and H&E stained sections. (a) Photoacoustic slice (along the red dashed line in Fig. 3(b)). Lines 1 and line 2 indicate the imaged dimensions along two different directions. (b) H&E stained section in the same position. Lines 1′ and line 2′ denote the measured dimensions in the H&E stained section. (c) Photograph of the tumor. All lines indicated by arrows in Fig. 4(a), Fig. 4(b) and Fig. 4(c) show the top margins of the tumor. (d). Transverse photoacoustic slice from another mouse. Lines 1 and line 2 indicate the imaged dimensions along two different directions. (e) H&E stained section in the same position. Lines 1′ and line 2′ present the actual dimensions in the H&E stained section. (f) Photograph of the tumor. All lines indicated by arrows in Fig. 4(d), Fig. 4(e) and Fig. 4(f) present the margins of the tumor in transverse plane. Scale bar, 500μm.

In another independent mouse tumor experiment, photoacoustic imaging demonstrated tumor nodules as shown in Fig. 4(d). The tumor size imaged by PAT along lines 1, and 2 (Fig. 4(d)) was 2.5 mm, 1.9 mm, showing an accurate measurement of the actual size of 2.5 mm, 2.1 mm, measured by histology along lines 1′ and 2′ (Fig. 4(e)). In this case, the largest observed error for the remaining two H&E sections was 9.5%.

Photoacoustic slices with histological correlations from the third mouse are shown in Figs. 5(a)-5(b). The structures indicated by the arrow in Fig. 5(b) are consistent with each other. After quantitative analysis, the largest observed error was 6.5%. Figures 5(c)-5(d) show the PAT slices and histological correlations for the fourth mouse where we added 1.1mm-thick chicken breast on top of the tumor to simulate the real specimen resected from the human breast. The 3D top margins of the tumor were clearly seen in the PAT images and consistent with the H&E sections. The white dashed line shows the surface of the chicken breast. The error between the PAT image and H&E sections was found to be less than 16.5%. A 1.8mm-thick chicken breast was added to the top of the fifth mouse and the PAT images with the associated H&E section are shown in Figs. 5(e)-5(f). The tumor shape imaged by PAT was close to that from the H&E sections but the error increased to 21.5% in this case.
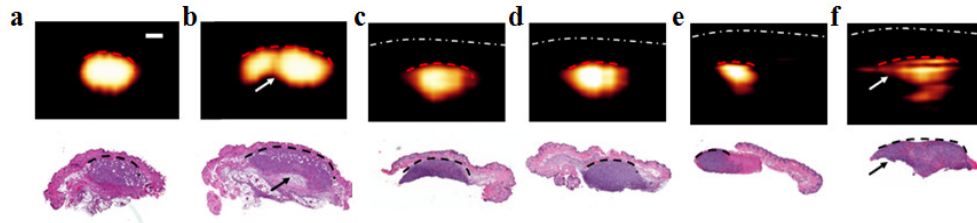
Fig. 5. Quantitative analysis of photoacoustic images in correlation with H&E sections with increasing image depth. (a,b) PAT slices and H&E sections for a tumor beneath the skin of mouse (0.3mm depth) . (c,d) PAT slices and H&E sections for a tumor beneath the mouse skin and a 1mm-thick chicken breast. (e.f) PAT slices and H&E sections for a tumor beneath the mouse skin and a 1.8mm-thick chicken breast. White dashed lines show the surface of chicken breast. Scale bar, 500μm.

4. Discussion

We have demonstrated that our iPAT technique with miniaturized MEMS probe can be effectively used for mapping tumors three-dimensionally and for inspecting completeness of tumor resection in small animals. The qualitative and quantitative results obtained are significant for several reasons. First, iPAT does not use any radioactive tracer or intravenous contrast. Second, the existing PAT techniques are not directly applicable to intraoperative imaging due to their bulky size or inflexibility of the imaging probe. Our MEMS-based probe breaks the limitation with its novel compact design. Third, after tumor resection, a surgeon can inspect the tumor cavity wall to ensure completeness of the procedure. Finally, iPAT has the potential to realize real-time image guidance and allow acquisition of functional parameters of tumor when a multispectral laser with high repetition frequency is used.

While our iPAT system has been demonstrated to be practical for intraoperative tumor imaging, several challenges still remain. First, a handheld probe is necessary for a surgeon to operate during surgery. In the current study, our probe was fixed in position using a holder and an aperture was used to generate a small light spot. In the future, we will use an optic fiber coupled with a micro-optical lens to replace the aperture and make the probe handheld. Second, imaging speed and area of our current iPAT system is limited by the 10 Hz repetition frequency of the laser source currently available in our lab. Considerably faster lasers (up to 5 kHz) are now commercially available. Since the resonant frequency of the MEMS mirror is up to 500 Hz, the imaging speed will be reduced to 5 s when a laser having a repetition frequency of 500 Hz is used. Third, the probe was submerged in a tank filled with water which is not applicable to clinical procedures. We plan to make a MEMS probe with a water- or ultrasound gel-filled balloon attached to the surface of transducer. Finally, the bleeding problem during a clinical surgery should be considered because the absorption of blood on 532nm is very strong. During the mouse experiments, we used cautery to stop the bleeding and normal saline to wash out the surgery area after tumor resection. For translating this technique to clinical applications, near-infrared pulsed laser should be used to avoid the strong affect from the bleeding and to increase the imaging depth. In this case, we will use tumor targeted contrast agent (e.g.,iron oxide nanoparticles) to provide enough contrast.

Acknowledgments